Ionics (2017) 23:427–433
DOI 10.1007/s11581-016-1860-5

ORIGINAL PAPER

Dependence of power density on anode functional layer thickness in anode-supported solid oxide fuel cells

Isao Kagomiya[1] · **Shunya Kaneko**[1] · **Yutaro Yagi**[1] · **Ken-ichi Kakimoto**[1] · **Kyeongsoon Park**[2] · **Ki-Hyun Cho**[3]

Received: 6 April 2016 / Revised: 1 October 2016 / Accepted: 8 October 2016 / Published online: 29 October 2016

Abstract To improve the power densities of anode-supported multilayer solid oxide fuel cells (SOFCs) based on an anode functional layer (AFL) and an anode support of Ni–YSZ (8 mol%Y_2O_3–ZrO_2), we systematically investigated how the AFL thickness influenced power density and impedance spectra, preparing the AFL using 65 wt% NiO–35 wt% YSZ with the anode support using 60 wt% NiO–40 wt% YSZ. Among the prepared SOFCs with AFL thicknesses from 0 to 100 μm, the ~10-μm-AFL SOFC (AFL10) showed the highest power density. Impedance spectroscopy of the prepared SOFCs was composed of an ohmic resistance as well as three constant phase elements (CPEs) resulting from activation- and concentration-polarizations. The impedance spectroscopy showed that AFL10 effectively decreased both the contact- and activation polarization-resistances. In addition, a part of the concentration polarization resistances for AFL10 was lower among the prepared SOFC samples. As such, AFL10 exhibited the highest power density among the prepared SOFC samples.

Keywords Anode-supported solid oxide fuel cells · Anode functional layers · Power density · Polarization resistances · Impedance spectroscopy

✉ Isao Kagomiya
kagomiya@nitech.ac.jp

[1] Life Science and Applied Chemistry, Nagoya Institute of Technology, Gokiso-cho, Showa-ku, Nagoya 466-8555, Japan

[2] Faculty of Nanotechnology and Advanced Materials Engineering, Sejong University, Seoul 143-747, Republic of Korea

[3] R&D Center, Samchun Pure Chemical Co., Pyeongtaek-si, Gyeonggi-do 440-3, Republic of Korea

Introduction

In anode-supported solid oxide fuel cells (SOFCs), a thinner electrolyte helps to produce a power density that is higher than in typical electrolyte-supported fuel cells [1–10]. However, in anode-supported cells, the anode support must be thick enough to provide sufficient mechanical strength for practical use, which increases the concentration polarization resistances and thus limits the power density [7].

An effective way to decrease concentration polarization resistances is to increase the porosity of the anode support. However, activation polarization resistance is inversely related to concentration polarization resistance. The activation polarization resistance increases with greater porosity or pore size. As demonstrated in several studies, one strategy to overcome these problems in anode-supported SOFCs is to introduce an anode functional layer (AFL) [7, 11–13].

In previous work, using tape-casting, we fabricated anode-supported multilayer SOFCs composed of LSM (cathode)/LSM-YSZ (cathode functional layer [CFL])/YSZ (electrolyte)/Ni–YSZ (anode support) with and without Ni–YSZ AFL, where LSM and YSZ are $La_{0.8}Sr_{0.2}MnO_3$ and 8 mol% Y_2O_3–ZrO_2, respectively [11]. Then, we prepared multilayer SOFCs with AFLs of various thicknesses. The SOFCs with an AFL had higher maximum power densities than those without an AFL. The AFL decreased the ohmic resistance because it promoted good electrical connection between the electrolyte and AFL. In addition, the increase in the three-phase-boundary (TPB) area decreased the activation polarization resistance. However, the concentration polarization resistance increased with the AFL thickness, because the AFL layer was denser than the anode support layer [11]. Park et al. reported similar effects of introducing an AFL in anode-supported SOFCs prepared with AFL thicknesses

of ~8, 19, and 24 μm [12]. However, they observed no remarkable dependence on AFL thickness.

Chen et al. also found similar effects of using an AFL in anode-supported SOFCs prepared with AFL thicknesses of approximately 5–15 μm [13], composed of 60 wt% NiO–40 wt% YSZ. The weight ratio between NiO and YSZ was the same in their AFLs as in their anode supports. In their experiment, the thicker AFL increased the ohmic resistance, which contrasted with our previous results [11]. We believe that this difference mainly comes from the weight ratio between NiO and YSZ in the AFL. Thus, AFLs in SOFCs have many important parameters, and the ideal AFL thickness and composition for producing high-performance cells remain unclear.

To better understand the influence of the AFL, the relationship between electrochemical properties and AFL thickness must be understood in a more systematic way over a wider range of thicknesses. With this in mind, here, we investigated how AFL thickness affected the electrochemical properties and power densities of SOFCs, where the AFL and the anode support were prepared using 65 wt% NiO–35 wt% YSZ and 60 wt% NiO–40 wt% YSZ, respectively. We chose to compare the power density of these SOFCs at 900 °C to simplify the polarization resistances. By measuring at 900 °C, we could neglect the polarization resistance of the cathode and CFL, as we will discuss later in this paper.

Experimental procedures

Preparation of anode-supported multilayer SOFCs by using tape-casting

Before preparing the single SOFCs, half cells (electrolyte/AFL/anode support) were prepared. The electrolyte was YSZ powder (8 mol%Y_2O_3–ZrO_2, 99.9 % purity, Tosoh Corp., Japan). The anode support used the same YSZ powder and NiO powder (99.9 % purity, Kishida Chem. Co., Ltd., Japan), mixed at NiO/YSZ = 60:40 wt%. As a pore-former, 50 vol% poly(methyl methacrylate) (PMMA; mean particle size = 1.5 μm; Soken Chem. Co., Ltd., Japan) was added to the YSZ–NiO powder. The PMMA was a more uniform particle size, making it easier to control porosity. The AFL was composed of 65 wt% NiO–35 wt% YSZ powder (Samchun Pure Chem. Co., Ltd., Korea), whose mean particle size was ~0.6 μm [11, 14].

The slurries for tape-casting were adjusted by mixing the powders with binder, plasticizer, and dispersant: an acrylic resin (OLYCOX, KC-7025T, Kyoeisha Chem. Co., Ltd., Japan), di-*n*-butyl phthalate (Kishida Chem. Co., Ltd., Japan), and FLOWLEN G-700 (Kyoei Chem. Co., Ltd., Japan), respectively. The slurries were tape-cast with a doctor blade (Imoto Seisakusho Co., Ltd., Japan). The obtained green sheets were cut to dimensions of 15 × 15 mm. The NiO–YSZ green sheets (for the anode support) and the YSZ green sheets (for the electrolyte) were stacked and then uniaxially pressed at ~13 MPa. In some samples, NiO–YSZ green sheets for the AFL were inserted between the electrolyte and anode support. After uniaxial pressing, the samples were subjected to cold isostatic pressing at 300 MPa. The pressed green samples were heated at 400 °C for 1 h in air to remove pore-formers and then co-sintered at 1300 °C for 3 h in air.

Using the obtained half cells, we prepared single SOFC cells. Raw powders of LSM ($La_{0.8}Sr_{0.2}MnO_3$; 99.9 % purity, Sigma-Aldrich Corp., USA) and YSZ (99.9 % purity, Tosoh Corp., Japan) were used to produce the CFL (50 wt% LSM–50 wt% YSZ) and the cathode (LSM). The slurries were made by mixing the cathode or CFL powder with carbon black, binder, and solvent.

The obtained slurry was screen-printed onto the half cells. The screen-printed LSM–YSZ and LSM were fired at 1250 °C for 2 h and at 1100 °C for 2 h, respectively. Then, a porous Pt electrode was deposited on both the cathode and anode, which were then fired at 930 °C. Before taking electrical measurements, we reduced the NiO in the AFL and anode support by heating it to 900 °C in an 8 % H_2–N_2 atmosphere. Table 1 gives the thickness of each layer in the prepared SOFCs. The AFL thickness was controlled in the range of 10–100 μm. Detailed preparation procedures are given in the literature [11].

Table 1 Thickness range of each layer of the prepared SOFCs.

Sample	Thickness (μm)				
	Anode support	AFL	Electrolyte	CFL	Cathode
AFL10	1000(100)	5–15	30–48	15–30	20–35
AFL20		15–25			
AFL40		40–60			
AFL60		60–80			
AFL80		80–100			

Characterization of the prepared SOFCs

The power densities of the prepared single cells were estimated from *I*–*V* curves measured in an atmosphere

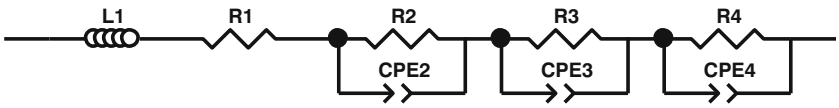

Fig. 1 Equivalent circuit used for impedance analysis of the anode-supported SOFCs

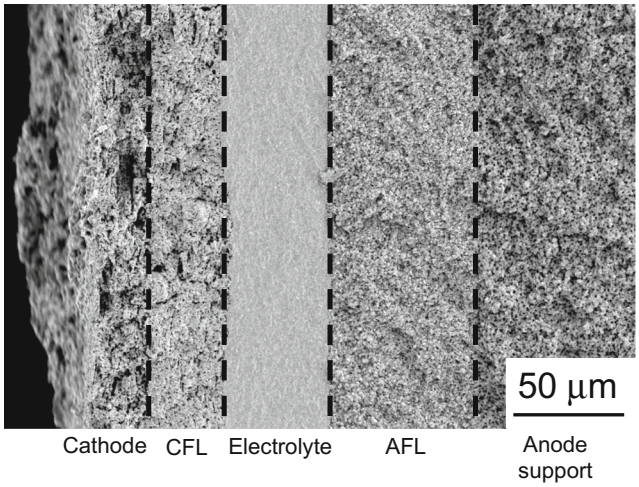

Fig. 2 Cross-sectional SEM image of the AFL60

gradient from 8 % H_2–N_2 (500 sccm) to air (500 sccm) by using a potentio-galvanostat (Princeton Applied Research VersaSTAT 3, Ametek Inc., USA). A Pyrex glass ring (AGC Techno Glass Co., Ltd., Japan) was located between the prepared SOFCs and the alumina tube and then fired at 900 °C to seal gas on the side of the reducing atmosphere. For these measurements, the current density was swept from 0 to 1.1 A cm^{-2}.

The prepared SOFCs were studied with impedance spectroscopy under an oxygen partial pressure gradient from 8 % H_2–N_2 (500 sccm) to air (500 sccm) by using a VersaSTAT 3 with an optional frequency response analyzer, sweeping the frequency from 5 MHz to 50 kHz. Both measurements were conducted at 900 °C without controlling for moisture content. To analyze the impedance spectra, we used the equivalent circuit depicted in Fig. 1, where $L1$ is an inductance, $R1$–$R4$ are resistances, and CPE2–CPE4 are constant phase elements. The impedance of a CPE (Z_{CPE}) is expressed as follows:

$$Z_{CPE} = \frac{1}{T(j\omega)^{\phi}} \quad (1)$$

where ω is the angular frequency, j is an imaginary number, T is a constant with units of F cm^{-1} $s^{\phi-1}$ related to capacitance, and ϕ is a parameter with a range of 0–1. When ϕ = 1, T corresponds to ideal capacitance [15]. The impedance spectra were fit to the equivalent circuit model by using Zview 3.4 software (Scribner Associates Inc., USA). Analyzing the differences in impedance spectra, we will later discuss the origins of the observed impedance resistances.

Results and discussion

Table 1 lists the thicknesses of each layer in the prepared SOFCs. As an example of the prepared SOFCs, Fig. 2 shows a cross-sectional SEM image of the AFL60 sample. This AFL was denser than that of anode support. It is difficult to investigate the actual porosities of the AFL and anode supports in the SOFCs, so we instead investigated the open porosities of isolated ceramics corresponding to the AFL and the anode support sintered in the same conditions. The open porosities of the isolated ceramic AFL and anode support were 26(1) and 42(2)%, respectively.

Figure 3 shows the I–V and power density curves at 900 °C. The open-circuit voltage (OCV) tended to increase with increasing AFL thickness, except for AFL40. Thickening the AFL decreases the local temperature near the electrolyte because of the larger distance between the electrolyte and the thermocouple, increasing the OCV, as discussed in the

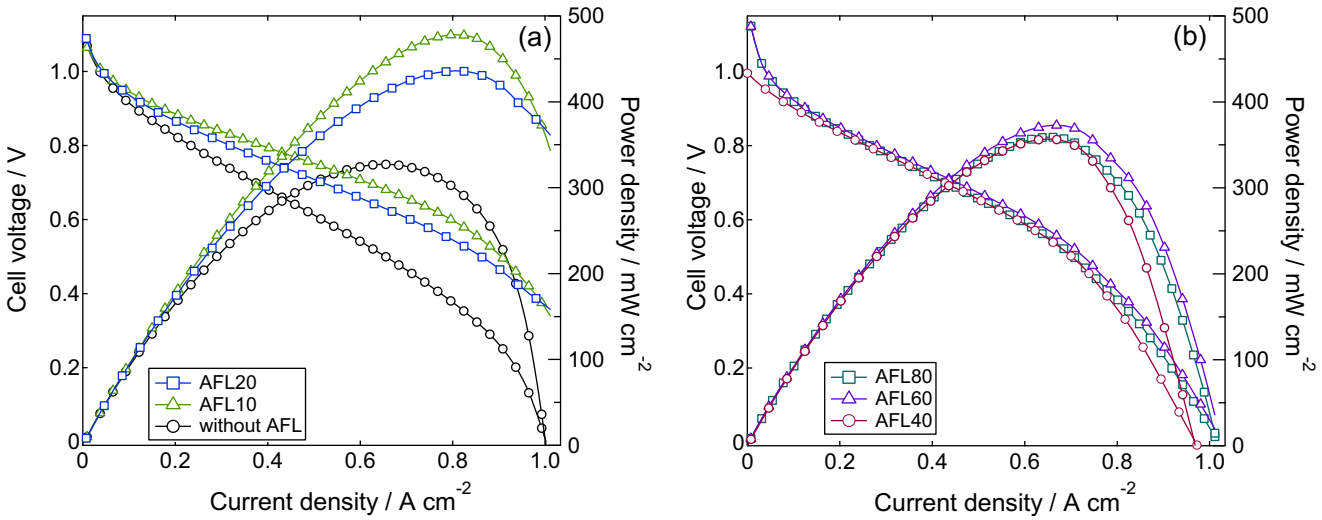

Fig. 3 I–V and power density curves of samples with the results for the no-AFL, AFL20, and AFL60 samples come from our previous report [11]

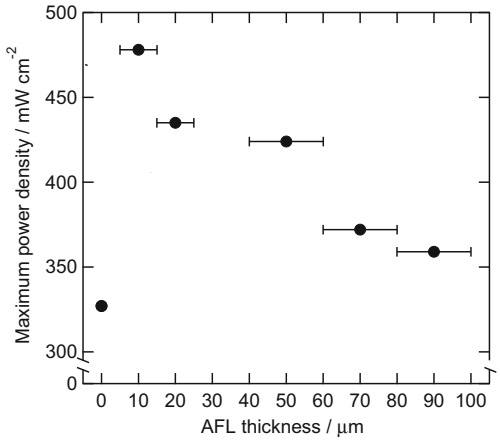

Fig. 4 Relation between AFL thickness and maximum power density for the prepared samples.

literature [13]. The smaller OCV for AFL40 may be related to the gas leakage, as discussed later.

The voltage drop after changing the current density from 0 to 1 A cm^{-2} for the AFL10 sample was smaller among the prepared samples with different AFL conditions. As a result, the maximum power density of AFL10 was 478 mW cm^{-2}, which was the highest among the prepared samples. As discussed later, the smaller voltage drop owes to the smaller activation- and concentration-polarization resistances.

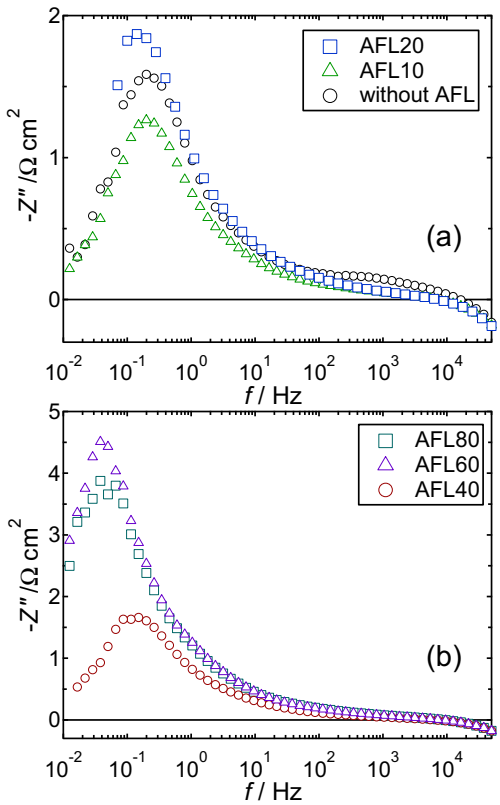

Fig. 5 Imaginary parts of impedance (Z″) versus frequency for samples. **a** No AFL, AFL10, AFL20. **b** AFL40, AFL60, AFL80

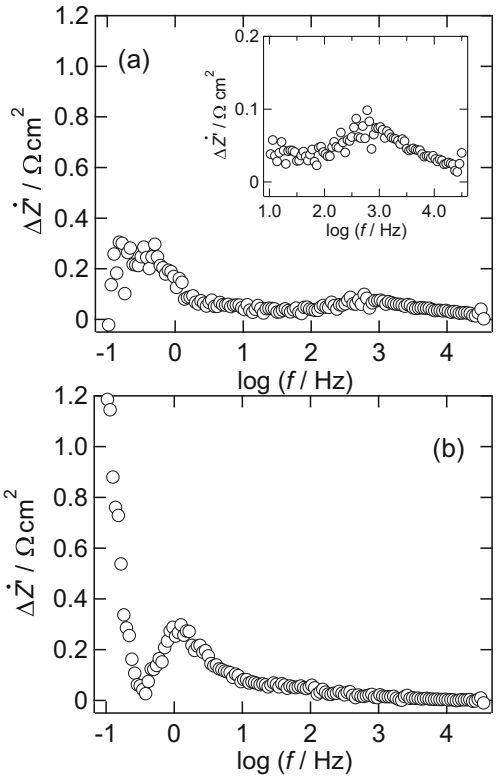

Fig. 6 Frequency dependence of **a** $\Delta\dot{Z}'$ between the no-AFL and AFL10 samples, and **b** $\Delta\dot{Z}'$ between the AFL10 and AFL80 samples

Figure 4 shows the relationship between AFL thickness and maximum power density, in which the maximum power density was estimated from the *I*–*V* curves at 900 °C. The maximum power density of AFL10 was higher than that of the no-AFL sample. As the AFL thickened further, the maximum power density gradually decreased. However, the maximum power density of AFL80 was still higher than that of the no-AFL sample.

Figure 5 plots the imaginary parts of impedance versus frequency. The no-AFL sample exhibited a large peak and a small, broad shoulder near 0.5 Hz and 10^3 Hz, respectively. The broad shoulder near 10^3 Hz seemed to disappear in AFL10 and AFL80. The peak near 0.5 Hz decreased in intensity for AFL10 and then increased gradually with thicker AFL. The peak position depended on the AFL thickness: for example, the peak shifted to a lower frequency in samples with thicker AFLs.

To further investigate the origin of the observed impedance, we estimated the difference in the impedance spectra $\Delta\dot{Z}'$ from the following equation [16, 17]:

$$\Delta Z'(f_n) \cong \frac{\left[Z'(f_{n+1}) - Z'(f_{n-1})\right]_{\alpha} - \left[Z'(f_{n+1}) - Z'(f_{n-1})\right]_{\alpha'}}{\ln(f_{n+1}) - \ln(f_{n-1})} \quad (2)$$

where f_n is a finite set of frequencies used for the impedance measurement, the index n is the number of the frequencies, Z' is the real part of Z, and α and α' are the operating conditions.

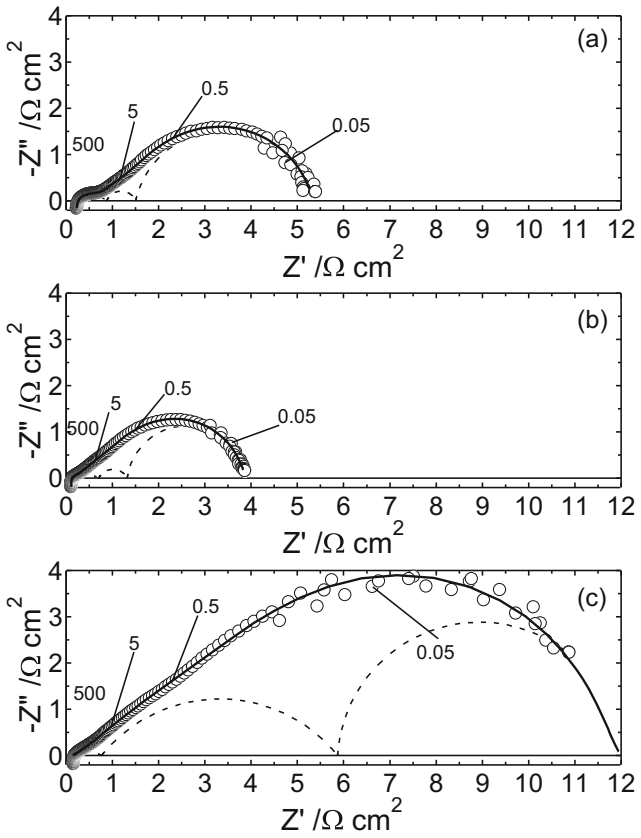

Fig. 7 Nyquist plots of the samples. **a** No AFL. **b** AFL10. **c** AFL80. The *open circles* are the investigated samples. The *solid lines* are patterns fit using the equivalent circuit in Fig. 1. The *dotted lines* are the fitted spectrum as the used individual arcs. The numbers indicate the measuring frequency (Hz)

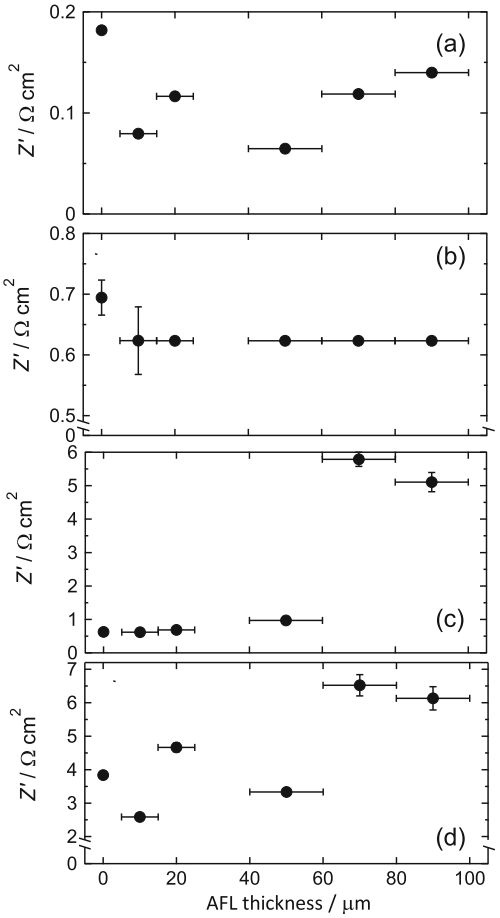

Fig. 8 Relationships between the AFL thickness and **a** *R*1, **b** *R*2, **c** *R*3, and **d** *R*4. The *vertical error bars* are estimated by fitting the observed Nyquist plots using the "Zview" program in Fig. 7. The *horizontal error bars* denote the samples' range of AFL thicknesses

A detailed explanation and analysis of the difference in impedance spectra can be found in the literature [16, 17].

Using Eq. (2), we can estimate how Z' changes by changing an operating condition. In this study, α and α' are different AFL thicknesses. Figure 6a shows $\Delta\dot{Z}'$. When α and α' are the no-AFL and AFL10 samples, respectively, three peaks appeared near 0.5, 1, and 10^3 Hz. The two peaks near 0.5 and 1 Hz overlapped considerably. This consideration is realized by comparing Fig. 6a with the case of Fig. 6b. When α and α' were AFL10 and AFL80, respectively, two peaks also appeared near 1 and 0.1 Hz (Fig. 6b). Note, however, that unreliable data were collected at frequencies below 0.1 Hz because of the larger noise signal. These peaks result from the presence of $\Delta\dot{Z}'$. The presence of $\Delta\dot{Z}'$ only came from changes in the AFL or anode support, because the CFLs and cathodes in the samples were the same.

As reported previously [16–18], three anode polarization resistances appeared. Note that the relaxation frequency of the polarizations depends on the gas composition on the anode side [18, 19]. Considering the literature, we believe that the broad peak observed at the highest frequency (~10^3 Hz in Fig. 6a) corresponds to the difference in activation polarization resistance between the no-AFL sample and the AFL10 sample because the relaxation frequency of activation polarization is much greater than that of concentration polarization, as discussed in the literature [16–19]. The activation polarization comes from a charge transfer reaction in the TPB. No peak appeared at ~10^3 Hz in Fig. 6b, meaning that the charge transfer electrochemical reaction rate in the TPB was the same in AFL10 and in AFL80. The other peaks below 1 Hz are related to modification of gas diffusion or gas transfer, owing to differences in AFL thickness.

Based on the previous discussion, we used the equivalent circuit of Fig. 1 to fit the investigated Nyquist plots. As shown by the solid line in Fig. 7, the investigated data (open circles) fit well to the equivalent circuit, where *R*1 is the ohmic resistance, *R*2 is the activation polarization resistance, and *R*3 and *R*4 are the concentration polarization resistances related to gas diffusion and gas transfer, as discussed before. *R*2, *R*3, and *R*4 contain considerable polarization resistance in the cathode, but the dominant resistances come from the anode support and the AFL because the resistances only depend on the

AFL conditions. Using the Nyquist plots of samples with various AFL thicknesses, we obtained $R1$, $R2$, $R3$, and $R4$, as shown in Fig. 8. Note that we made the $R2$ for AFL20, AFL40, AFL60, and AFL80 equal to the $R2$ of AFL10 because AFL10 and AFL80 have the same activation polarization resistance, as described before.

Inserting the AFL abruptly decreased $R1$ because the contact resistance between the AFL and electrolyte is lower than that between the anode support and electrolyte, owing to the higher electrical conductivity of the AFL. The higher electrical conductivity of the AFL comes from the NiO–YSZ composition of 65:35 wt%. $R1$ intended to increase with thicker AFL, suggesting the thicker AFL increase the total ohmic resistance in the SOFCs.

The $R2$ in the no-AFL sample was larger than in the samples with AFLs, meaning that inserting the AFL effectively decreased the activation polarization resistance, caused by the greater TPB area. As mentioned before, we believe there are no notable differences in $R2$ among the samples with various AFL thicknesses. For the prepared SOFCs, the activation polarization resistance in the TPB is mainly limited in the interface between the electrolytes and the AFLs.

As the AFL thickness increased from the no-AFL sample to the AFL40 sample, $R3$ slightly increased but then abruptly increased as the thickness increased further. This trend means that the thicker AFLs prevented gas diffusion and transfer because these AFLs were denser than the anode support, as mentioned before.

Because $R4$ increased with AFL thickness, $R4$ is also related to gas diffusion and transfer. However, $R4$ in the AFL10 sample was lower than in the no-AFL sample, suggesting that more active charge transfer in the TPB also hasten gas diffusion and transfer. Note that the OCV of AFL40 was smaller than in the other prepared samples. The $R4$ of AFL40 was smaller than in AFL20, AFL60, and AFL80. These results suggest that gas leakage in AFL40 decreased its OCV and $R4$. A detailed investigation of the relations between AFL thickness and gas leakage or microcracking in the cell preparation conditions remains for future study.

From these results, the AFL10 sample showed the best cell performance because it had the lowest activation polarization resistance and lowest concentration resistance $R4$ among the samples. Our results suggest that the cell performance can be further improved by thinning the AFL further, which is the next step of this study.

Figure 9 summarizes the refined parameters of T and ϕ for each CPE. As shown in Fig. 9a, inserting the AFL increased T remarkably, meaning that it decreased the imaginary part of

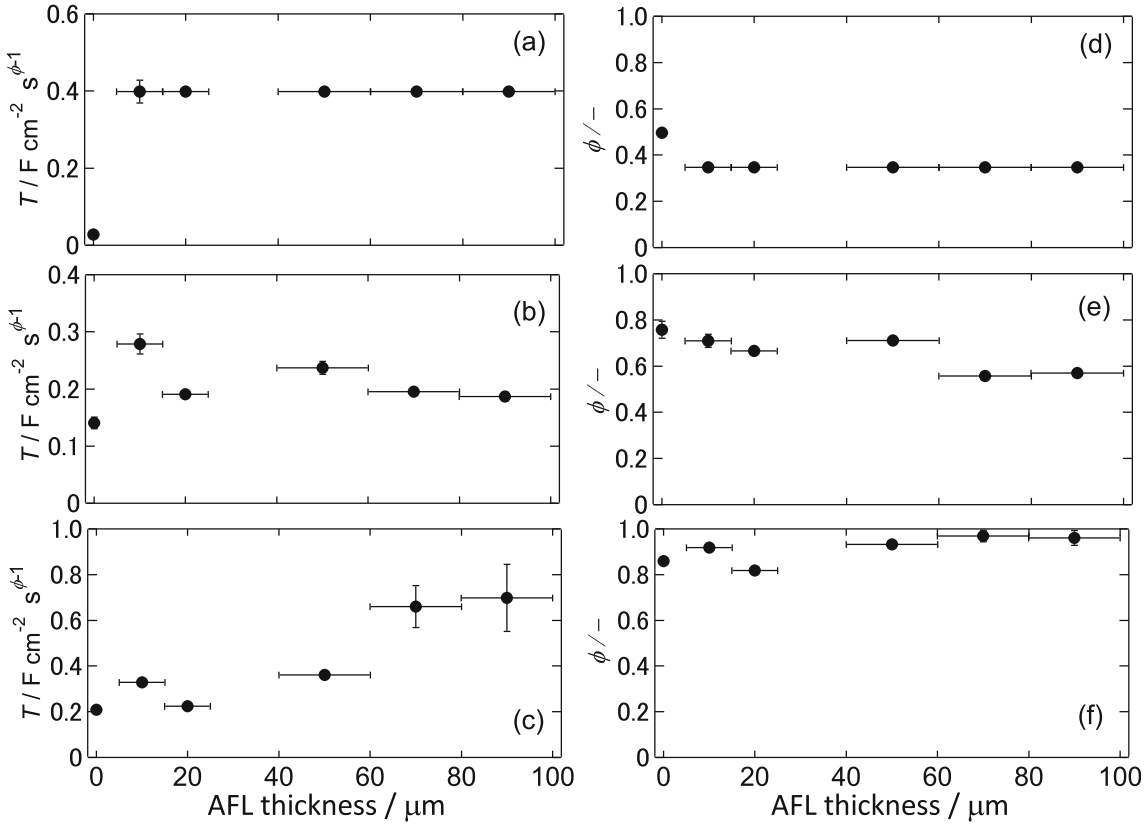

Fig. 9 Relationships between the AFL thickness and T of **a** CPE2, **b** CPE3, and **c** CPE4. Relationships between the AFL thickness and ϕ of **d** CPE2, **e** CPE3, and **f** CPE4.The *vertical error bars* are estimated by fitting the observed Nyquist plots using the "Zview" program in Fig. 7. The *horizontal error bars* denote the samples' range of AFL thicknesses.

the impedance ($-Z''$). This is comparable with the results in Figs. 5 and 7. The T in CPE3 of samples with AFLs was greater than that of the no-AFL sample. As the AFL thickened, T in CPE4 gradually increased. A ϕ of less than unity means that the relaxation times of each polarization are widely distributed. Based on Fig. 9d–f, the relaxation time related to activation polarization has a wider distribution than that related to concentration polarization.

The approach of this study would be also effective to investigate the effect of AFL thickness in anode-supported SOFCs at intermediate temperature range of 600–800 °C, remaining as the future study.

Conclusions

Using tape-casting, we prepared anode-supported multilayer SOFCs of LSM/CFL/YSZ/Ni–YSZ with and without AFLs of various thicknesses, approximately 10 to 100 μm. The AFL and the anode support were composed of 65 wt% NiO-35 wt% YSZ and 60 wt% NiO-40 wt% YSZ, respectively. We investigated how the AFL influenced the cell performance and electrochemical properties. Among the samples, the SOFC with an AFL thickness of ~10 μm showed the highest power density. Impedance analysis showed that the AFL10 sample effectively decreased both the contact and activation polarization resistances ($R1$ and $R2$). In addition, the AFL10 sample had a lower $R4$ concentration polarization resistance, while keeping a similar $R3$ concentration polarization resistance.

Acknowledgments This study was partially supported by the Korea Association of Industry, Academy and Research Institute (KAIARI).

References

1. Leng YJ, Chan SH, Khor KA, Jiang SP, Cheang P (2003) Effect of characteristics of Y_2O_3/ZrO_2 powders on fabrication of anode-supported solid oxide fuel cells. J Power Sources 117:26–34
2. Leng YJ, Chan SH, Jiang SP, Khor KA (2004) Low-temperature SOFC with thin film GDC electrolyte prepared in situ by solid-state reaction. Sol Stat Ion 170:9–15
3. Mai A, Haanappel Vincent AC, Tietz F, Stöver D (2005) Ferrite-based perovskites as cathode materials for anode-supported solid oxide fuel cells: part I. Variation of composition. Sol Stat Ion 176: 1341–1350
4. Perednis D, Gauckler LJ (2004) Solid oxide fuel cells with electrolytes prepared via spray pyrolysis. Sol Stat Ion 166:229–239
5. Nguyen TL, Kobayashi K, Honda T, Kato T (2004) Preparation and evaluation of doped ceria interlayer on supported stabilized zirconia electrolyte SOFCs by wet ceramic processes. Sol Stat Ion 174:163–174
6. Wang Z, Qian J, Cao J, Wang S, Wen T (2007) A study of multilayer tape casting method for anode-supported planar type solid oxide fuel cells (SOFCs). J Alloys Comp 437:264–268
7. Yang S, Chen T, Wang Y, Peng Z, Guo W, Wang WG (2013) Electrochemical analysis of an anode-supported SOFC. Int J Electrochem Sci 8:2330–2344
8. Kim SD, Lee JJ, Moon H, Hyun SH, Moon J, Kim J, Lee HW (2007) Effects of anode and electrolyte microstructures on performance of solid oxide fuel cells. J Power Sources 169:265–270
9. Wu W, Wang X, Liu Z, Zhao Z, Ou D, Tu B, Cheng M (2014) Influence of deposition temperature of GDC interlayer deposited by RF magnetron sputtering on anode-supported SOFC. Fuel Cells 14: 171–176
10. Menzler NH, Malzbender J, Schoderbçck P, Kauert R, Buchkremer HP (2014) Sequential tape casting of anode-supported solid oxide fuel cells. Fuel Cells 14:96–106
11. Kagomiya I, Kaneko S, Kakimoto K, Park K, Cho KH (2015) Fabrication and power densities of anode-supported solid oxide fuel cells with different Ni-YSZ anode functional layer thicknesses. Fuel Cells 15:90–97
12. Park YM, Lee HJ, Bae HY, Ahn JS, Kim H (2012) Effect of anode thickness on impedance response of anode-supported solid oxide fuel cells. Int J Hydrog Energy 37:4394–4400
13. Chen K, Chen X, Lü Z, Ai N, Huang X, Su W (2008) Performance of an anode-supported SOFC with anode functional layers. Electrochim Acta 53:7825–7830
14. Kim J, Cho KH, Kagomiya I, Park K (2013) Structural studies of porous Ni/YSZ cermets fabricated by the solid-state reaction method. Ceram Int 39:7467–7474
15. Jorcin JB, Mark Orazem ME, Pébère N, Tribollet B (2006) CPE analysis by local electrochemical impedance spectroscopy. Electrochim Acta 51:1473–1479
16. Jensen SH, Hjelm J, Hagen A, Mongensen M (2010) Electrochemical impedance spectroscopy as diagnostic tool, Handbook of fuel cells—Fundamentals, Technology and Applications. Wiley, New York
17. Barfod R, Mongensen M, Klemenso T, Hagen A, Liu YL, Hendriksen PV (2007) Detailed chracterization of anode-supported SOFCs by impedance spectroscopy. J Electrochem Soc 154:B371–B378
18. Mohammadi R, Ghassemi M, Mollayi BY, Pirkandi J (2014) The effect of mass transfer on electrochemical impedance of a solid oxide fuel cell anode. J Sol Stat Electrochem 18:2815–2827
19. Nakajima H (2010) Electrochemical impedance spectroscopy study of the mass transfer in an anode-supported microtubular solid oxide fuel cell. In: Nakajima H (ed) Mass Transfer–Advanced Aspects. InTech, Rijeka, Croatia, pp 285–304.